Digital Material Design Using Tensor-based Error Diffusion for Additive Manufacturing

Yuen-Shan Leung[a], Tsz-Ho Kwok[b], Huachao Mao[a], Yong Chen[a,*]

[a]Epstein Department of Industrial and Systems Engineering, University of Southern California, USA

[b]Department of Mechanical, Industrial and Aerospace Engineering, Concordia University, Canada

Abstract

Recent multi-material additive manufacturing (AM) technologies enable the fabrication of an object with accurate deposition of different types of materials. Hence, in addition to geometric shapes, it is possible to use different material compositions to optimize the mechanical properties of a component for given design requirements. However, current AM processes have a limitation on the number of materials that can be deposited during the fabrication process. Due to the constraint, it is critical to optimize the material distribution using the limited base materials; however, an extremely large design space exists in a design domain that is enabled by the AM technologies. In this paper, we introduce a digital material design framework to generate digital material compositions that can be printed and be able to achieve the desired behavior. We take analog material composition as the input and perform the analog-to-digital conversion using an exemplar-based approach based on a pre-computed material library. The patterns in the library are constructed with different combinations of the given base materials, and their mechanical properties are computed using finite element simulation. Accordingly, the design goal of the analog-to-digital conversion is to find material composition in the design domain with matching mechanical properties. A tensor-based error diffusion algorithm has been developed to reduce the approximation error during the conversion effectively. Experimental tests based on the design framework have been performed. The test results demonstrate our framework can quickly find effective solutions for various multi-material design problems.

Keywords: Additive manufacturing; Digital material design; Error diffusion; Tensor; Robotic grasper.

1. Introduction

Additive manufacturing (AM), a.k.a. three-dimensional (3D) printing, is capable of using multiple types of materials to fabricate heterogeneous objects [1] [2]. Its layer-based fabrication strategy allows the controlled deposition of different materials in a single object during the fabrication of each layer. Currently, several multi-material AM processes have been developed that can print heterogeneous objects (HO), including multiple-nozzle deposition [3], multiple-powder deposition [4], multiple-droplet dispensing [5], and multiple-vat-based polymerization [6]. In a multi-material AM process such as multiple-vat-based polymerization, a 3D model is first sliced into a set of cross-sectional two-dimensional (2D) images to control the solidification of different photocurable resins in a layer. Because of the accurate material deposition capability in the layer-based multi-material AM process, tremendous design flexibility is provided in defining heterogeneous material composition in a computer-aided design (CAD) model. Hence, in addition to geometric shapes, designers can now refine and optimize material distributions in a product component to meet design requirements. Varying material distribution in an object may also help designers to address a broader spectrum of design challenges [7]. For example, a tweezers fabricated from a single material as shown in Fig. 1(a) has a grasp force that is proportional to the input force; for an input force of 5 N, the grasp force would be 2.5 N. Such a force may be too large to grasp a fragile object such as a pill or a cell. To avoid the added force to crush the object, assume a maximum grasp force is given (e.g., 0.3N). The tweezers based on a single material will require the user to apply a very small force or to incorporate an additional mechanism in the design to control the added force by the user. Such a design challenge can

---

* Corresponding author.
E-mail address:yongchen@usc.edu

easily be addressed by altering the material properties throughout the tweezers to change the relationship between the applied force and the grasp force. For example, a design with the continuous material distribution expressed by Young's modulus is shown in Fig. 1(b). Without changing the geometric shape of the tweezers, the multi-material design can achieve 10x smaller grasp force based on simulation [7].
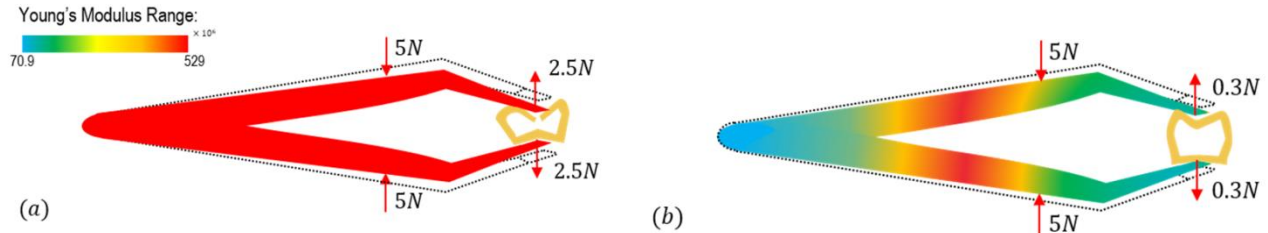
Fig. 1. (a) When a tweezers with a default material is used, the normal contact force is so large that may break a fragile object; (b) a customized material distribution is favorable for this case leading to a lower contact force with the same applied force. However, the design cannot be fabricated by the existing 3D printing technologies. This paper aims at converting the continuous material composition into a manufacturable design for multi-material AM technologies.

Although objects with continuously varying material properties (called analog material composition in the paper) can accurately achieve desired mechanical performance, none of multi-material AM technology can fabricate such an object with analog material composition, since its fabrication requires a very large number of materials. The digital printing concept [6] [8] [9] using a voxel-based representation enables digital material composition to be fabricated by AM processes. That is, an object can be decomposed into many assembled voxels, and a multi-material AM machine can be used to control the deposition of limited types of base materials in the voxel domain. The deposited material in each voxel is homogeneous instead of continuously varying. Directly using the available digital materials to compute the material composition with desired material properties is an optimization problem, in which the material variables in the design domain are discrete integers. The optimization of material composition is an integer programming problem, which is known to be NP-hard. Even with a limited number of based materials (e.g., 2-4), the design space of the digital material composition defined on voxels is extremely large. For example, for a simple cubic model represented by $100 \times 100 \times 100$ voxels and only two base materials, there would be 2^{1e6} of possible combinations that need to be considered. Hence, for a given design requirement, how to optimize digital material composition is very challenging due to the extremely large design space that is discrete. The goal of this paper is to present a new design methodology for computing digital material composition using an analog-to-digital material converter.

Recently a fast multi-material design approach [10] based on analog material composition has been developed for 3D volumetric meshes. Our design framework takes such analog materials composition as the input. The main focus of the paper is to develop an analog-to-digital material conversion so that an accordingly designed multi-material component can be 3D-printed using a few base materials and can achieve a similar design behavior. In other words, to address the challenging problem of optimizing digital material composition to achieve a given design requirement, we will utilize the analog material composition as underlying guidance in computing a 3D-printable design that only consists of the available base materials that are defined on a set of voxels. In our approach, the whole design domain is subdivided into a set of tiles, and the analog-to-digital material conversion on each tile is implemented through the search of the closest pattern from a digital material library, which was pre-constructed using finite element analysis (FEA) for a given AM technology. The searching of the closest pattern and the related error diffusion are done by considering the mechanical properties of a tile. Our contributions are summarized as follows.

- An exemplar-based approach has been developed that makes use of the analog material composition as guidance to generate digital material composition. The method subdivides a design domain into a set of voxels and tiles whose material depositions can be determined based on the pre-computed digital material library.
- To compare the mechanical properties of heterogeneous tiles, a tensor representation to describe the deformation behavior has been developed to enable the search of the closes pattern from the digital material library.
- A novel error-diffusion algorithm has been introduced to propagate and minimize the approximation errors of digital material composition in terms of mechanical properties of the accordingly printed heterogeneous object.

In our research work, we demonstrated the use of a small number of base materials to approximate the mechanical properties of analog material composition closely. We validated our results through both simulation and physical experiments on multiple test cases. Although the HO fabrication in our tests was carried out using the multi-vat-based polymerization process [6], our approach can be applied to other multi-material AM processes. For the challenging problem of digital material design to achieve prescribed design performance, our work is a proof-of-concept that may present a research path for the exploration of optimal HO solutions for future engineering systems. The rest of the paper is organized as follows. Section 2 reviews the related

works. Section 3 presents the algorithm overview. The implementation details are discussed in section 4. The experimental results are presented in Section 5. Finally, section 6 concludes the paper with future works.

2. Related Work

Since the capability of designing digital material composition with specified elastic property is the focus of the paper, we review the literature related to varying mechanical properties of materials in this section.

Structural Design. Micro-structured material can be seen as a new material with totally different mechanical properties [11]. Sigmund *et al.* [12] introduced a method to design the periodic microstructure of a material to obtain prescribed constitutive properties. They formulated the problem of finding the simplest possible microstructure to achieve desired elastic properties as an optimization problem named inverse homogenization problem. Since then, much progress has been made in developing and identifying microstructures with desired behaviors [13, 14, 15]. These microstructures can be obtained using various topology optimization algorithms, such as the homogenization method [16], the solid isotropic material with penalization (SIMP) [17], and the level-set method [18]. However, topology optimization (TO) is an iterative approach that performs FEA repeatedly until the best solution is found. Recently some non-iterative and fast approaches for optimal structure design have also been developed [19]. The TO process typically results in high computational efforts, especially for a design domain that requires a fine resolution. Bickel *et al.* [19] presented a method to measure deformations of base material's structures and stack them to reach a target behavior through combinatorial optimization. Schumacher *et al.* [21] extended this idea by designing microstructure to match given homogenous material properties. These microstructures are tiled to create objects with spatially varying elastic properties. On the other hand, Panetta *et al.* [21] introduced a library of tileable parameterized 3D microstructures to control the elastic material properties of an object. By choosing a space of structures with a limited but sufficiently large set of parameters, a small family of structures can be optimized to achieve specific material properties. However, the boundary matching problem between the neighboring tiles must be handled carefully. Also, some fabrication constraints (e.g., avoid supporting structures) need to be considered. A recent work [22] presented a framework to optimize the structure and material distribution of an object based on given design specifications. The authors utilized multi-material microstructures to map the optimal material properties with the corresponding properties so that the objects with prescribed functional performances can be fabricated. Different from their work, the proposed method is a direct digital material design approach that avoids the burden of high-dimensional optimization.

Material Design. Heterogeneous objects that comprise two or more materials have been widely used in engineering systems to achieve desired performances. HO offer an advantage over homogeneous objects since their functionality can be satisfied by designing the material variations in the objects. Some research has been done for modeling and representing a heterogeneous object so that the flexibility of controlling both the material distributions and geometric shape design is allowed. For example, several mesh-based approaches [23, 24] were presented to represent functionally graded material objects. They decomposed a HO model into finite elements and offered local control on material composition. However, these methods show limitations due to the approximation of geometry. To address the issue, the feature-based approaches [25, 26, 27] have been introduced to relate material composition with design features directly. These methods have enabled a HO to exhibit different properties by using features that play a key role in defining the object's performance. To form a HO with target behaviors, its material properties must be determined first. Various designing approaches for modeling heterogeneous objects have been developed in the field of computer graphics. For accurately modeling deformable materials, one popular way is to use continuum elasticity laws together with finite element modeling. By selecting a proper constitutive material model and tuning its parameters, a large range of materials can be modeled, including those with nonlinear and heterogeneous deformation behavior. Also, methods to estimate material parameters of the constitutive model have been proposed such as considering Young's modulus alone [28] and Young's modulus with Poisson ratio [29]. Recent works on acquiring complex heterogeneous deformation were developed through either a data-driven modeling approach [30] or a material distribution optimization approach [10]. However, these design approaches are not fabricated-oriented. To fabricate smooth heterogeneous objects using a limited number of materials, 3D halftoning using error diffusion filters [31, 32] and dithering method [33, 34] have been employed before. Yet, none of these approaches have provided a general fabrication-oriented design approach to generate digital material composition for AM technologies that can achieve target behavior.

3. Definition and Algorithm

An object with multi-material compositions can bring tremendous design freedoms that may enable a HO to achieve performances that were difficult to achieve using a single material. However, how to design a heterogeneous object that can be fabricated by current multi-material AM processes and achieve given design performance at the same time is still an open question. Directly optimizing digital material composition using the given base materials is a mixed-integer optimization

problem, which is well-known difficult and NP-hard. Our framework makes use of the previously developed multi-material design approach [10] that uses tetrahedron meshes as design elements to speed up the optimization process. The computed analog material composition can satisfy the user's specified deformation behavior at specified locations. Based on the analog material design result, we compute the related digital material composition that has similar deformation behavior and, more importantly, is 3D-printable by the current AM technologies.

One important assumption underlying the use of our design framework is that the spatial distribution of base materials can generate intermediate mechanical properties of these materials. This assumption has been physically validated by Huang *et al.* [9], allowing our design framework to be directly used to address real-world problems. Without the loss of generality, our discussion focuses on 2.5D cases for the sake of simplicity. A similar method can be extended to 3D cases as discussed in future work (Section 6). Given a 2D domain Ω of arbitrary shape, we discretize the domain into finite elements of squares and group them into a set of tiles. Assume each tile is a 3-by-3 grid of elements denoted as C. Each of the elements is associated with a designated Young's modulus. Hence the problem considered in this research is defined as follows:

For a query tile C made of m materials, find a tile L that can best-approximate the mechanical property of C, where L is made of k materials and $m \gg k$.

To solve the problem, we propose an exemplar-based framework (shown in Fig. 2) that consists of both offline and online phases. In the offline phase exemplars of material compositions are created to build a digital material library, and in the online phase, the best pattern is searched from the library to closely match the behavior of a queried tile with continuously varying materials properties.
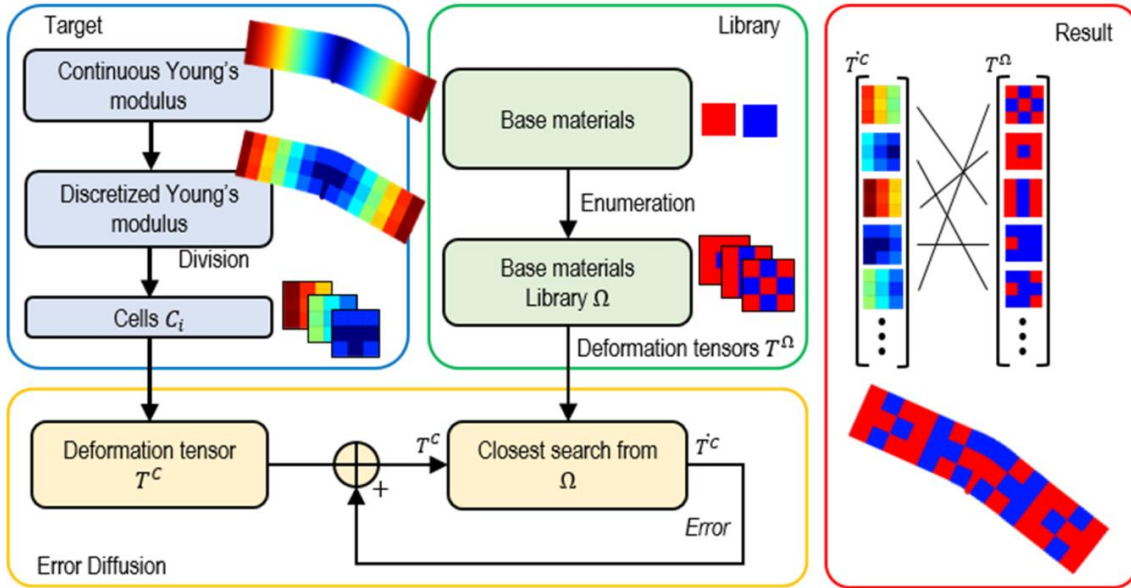

Fig. 2. Overview of our design framework.

The matching of the materials in a local region by "average" properties (e.g., Young's modulus) has been applied in computer graphics [35] and fabrication [20]. However, it is not accurate enough because Young's modulus does not follow a linear relationship with the material composition. The error would be large when the material properties of the base materials in the structure differ vastly. Hence searching and matching material patterns with average properties may lead to significant errors when the material property differences between the base materials are large [9]. In this paper, we define a tensor T^C and propose using it to describe the mechanical property of a tile C. The tensor contains the longitudinal and transverse deformations incurred by normal stresses σ and shear stresses τ. Hence, compared with using simple properties such as Young's modulus, tensor T^C can be better similarity measurement criteria when searching and matching material compositions. The presented search approach based on tensors is a novel use of the explicit behavior matching in finding a close match to a target material property. The tensor T^C is defined as follows.

3.1 Tensor Definition

Given a square 3×3 grid with 4×4 nodes and made of m linear elastic materials, the tensor T^C is defined by four independent components: e_{xx}, e_{yy}, e_{xy} and e_{yx}. The e_{xx} and e_{yy} represent the deformations subjected to axial tensile forces, while the e_{xy} and e_{yx} represent the deformations subjected to axial shear forces as illustrated in Fig. 3(b). Both Young's modulus and Poisson's ratio v can vary in the tile. In response to the applied loads, deformations can be expressed in functions of x and y. Considering all elements in the tile as a whole, our main interest is the explicit behaviors on element boundaries. Hence we can concatenate the deformations on the 4×4 nodes to form vectors, which can be defined as follow:

$$T^C = \begin{bmatrix} e_{xx}(3,0) & e_{xx}(3,1) & e_{xx}(3,2) & e_{xx}(3,3) \\ e_{yy}(0,3) & e_{yy}(1,3) & e_{yy}(2,3) & e_{yy}(3,3) \\ e_{yx}(3,0) & e_{yx}(3,1) & e_{yx}(3,2) & e_{yx}(3,3) \\ e_{xy}(0,3) & e_{xy}(1,3) & e_{xy}(2,3) & e_{xy}(3,3) \end{bmatrix} \tag{1}$$

where the index (i,j) corresponds to the node index in the grid, and each deformation vector is determined by the nodal displacement. For example, the element $e_{xx}(3,2)$ is derived at node $n(3,2)$ in Fig. 3(a), where the line is subjected to a force acting in the x-direction. The amount of elongation depends upon the displacement at nodes $n(0,2)$ and $n(3,2)$. If the end node displaces $d(3,2)$ and the start node displaces $d(0,2)$, the deformation $e_{xx}(3,2)$ is equal to $d(3,2) - d(0,2)$. Each node along the boundary captures a unique response of the tile to a load. Hence by combining them together, a material property identification can be created for tile C. We used finite element structural analysis to calculate the nodal displacements in order to compute the tensor information. The result is a combination of both shear and tensile strains that capture the characteristics of the tile. Four boundary conditions are used for four components (as shown in Fig. 3(b)) and each component represents the deformation state in a single DOF that satisfy the boundary conditions. Therefore they can be independently computed and combined to construct tensor T^C. With the definitions of the problem and the tensor, the implementation of our digital material design framework will be discussed in Section 4.
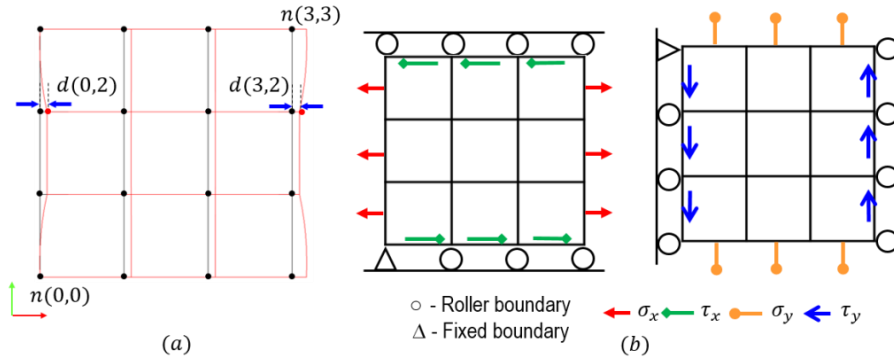
Fig. 3. (a) Element $e_{xx}(3,2)$ of deformation vector e_{xx} is derived from two node points. (b) Four boundary conditions (represented in four types of arrow) are applied on a tile to extract the corresponding behavior.

4. Implementation

To approximate an arbitrary material distribution of k base materials, we propose an exemplar-based framework to enable a direct digital material design by subdividing the whole design domain into a set of tiles. Accordingly, the framework consists of an offline phase to generate the exemplar tiles in a digital material library and an online phase to search and match a queried tile from the library.

4.1 Offline Process

As a pre-processing step, the offline phase consists of constructing a digital material library with k base materials to enumerate the possible spatially distributed patterns from such materials. Each pattern is defined by a n-by-n unit-square grid. Elements in the grid are assigned with one of the base materials such that every grid forms a unique pattern in the library. The digital material library is a collection of tiles that made up of two or more isotropic materials, where each tile can have various behaviors when subjected to external forces. The tile can be defined with different size n ($n \geq 2$). A large size n results in an exponential growth of library size and the stresses experienced by the tile are more complicated that may result in a larger

approximation error, while a small size n results in fewer degrees of freedom with simpler stress conditions when finding a close approximation from the library. As a balance between the quality, the simplicity, and the efficiency, a 3-by-3 tile ($n = 3$) is selected in this research. Suppose there are 2 base materials (i.e., $k = 2$, M_{soft} and M_{hard}) provided by a multi-material AM machine. The flexibility of the two materials could have over 100× difference. Accordingly, the number of the patterns in the digital material library is $k^{n \times n} = 512$. We enumerated all the possible patterns by changing the number and the position of the two base materials. For example, if 3 soft elements and 6 hard elements are placed in one tile, we can have 84 different patterns for all the combinations, which is an *n-choose-k* problem. A tensor T^L (L stands for a tile in library) is then computed to describe the mechanical property of the related tile. We employ the k-d tree data structure to store the result so that this high-dimensional search in the online phase can be sped up.

4.2 Online Process

In the online phase, the input analog material composition is quickly converted into the related digital material composition. An input model with continuous material composition is first voxelized into cubic block elements. In the analog-to-digital conversion, it is always preferred to use a higher resolution so that the approximation error can be smaller. However, limited by the physical constraints, the resolution of a voxel needs to be setbased on the fabrication resolution of the used 3D printer. As the element size is small and the material distribution in an object is smooth, the Young's modulus of each element can be represented by the value of the input continuous material distribution at its centroid point. Accordingly, tiles are generated from the voxels and approximated by the exemplars in the digital material library.

Tile Generation. In solving the material distribution problem, the domain Ω is divided into tiles. Each tile is a 3-by-3 grid that is the same as the ones that were used in constructing the offline library. A tensor T^C is associated with the tile C describing the deformation behavior of the subdomain. Tensors are extracted for all the tiles with the same loading and boundary conditions as the ones used in the offline phase. While the tiles in the library are squares, the tiles in the object maybe irregular especially for an object with freeform shapes. That is, when the boundary of the domain $\partial\Omega$ is not straight, the related tiles contain empty elements inside. During the matching process, we fill the empty elements by M_{soft}. This is because the soft elastic material has a minimum effect on the deformation of other elements, and the empty elements are more likely to be assigned as soft material. After finishing the matching process, the elements filled by M_{soft} will be reassigned as empty and no material will be deposited to empty elements during fabrication.

Similarity Measures for Tensors. We aim to find a deformation tensor T^L from the library that maps the corresponding tile L onto the target tile C by minimizing the objective function:

$$\epsilon(C) = \epsilon_{sim}(T^C, T^L) \tag{2}$$

where ϵ_{sim} stands for the distance measure between two tensors. The similarity is measured by the Frobenius norm of the distance between the tensors T^C and T^Ls, i.e., $\underset{i}{\arg\min} \|T^C - T_i^L\|_F$, where i is the index for the samples in the library. The tensor distance, ϵ_{sim}, between two tensors T^C and T^L is given by

$$\epsilon_{sim} = \|A\| = \left(\sum_{i=1}^{4} \sum_{j=1}^{4} |a_{ij}|^2 \right)^{\frac{1}{2}} \tag{3}$$

where

$$A = T^C - T^L,$$

and

$$A = \begin{bmatrix} e_{xx}^C(3,0) - e_{xx}^L(3,0) & \cdots & e_{xx}^C(3,3) - e_{xx}^L(3,3) \\ \vdots & \ddots & \vdots \\ e_{xy}^C(0,3) - e_{xy}^L(0,3) & \cdots & e_{xy}^C(3,3) - e_{xy}^L(3,3) \end{bmatrix}$$

In this way, the tile is treated as though it has undergone multi-axial states of stresses during the comparison. The approach individually captures four loading responses for each tile and combines them all to determine the dissimilarity between any two tiles. For example, the tensor matching results of all the tiles in a L-shaped slot (refer to the test case in Fig. 10) are shown in Fig. 4. For each tile, the closest digital material pattern was identified in the library based on the similarity measures and the related error was calculated. As shown in Fig. 4, most tiles show small errors. One of the tiles with a large error is shown in Fig. 4. The target material distribution has Young's modulus ranging from 1.13e8 to 1.22e8. The digital material pattern using the based materials with Young's modulus of 2e6 and 2.5e8 to match the given tile is also shown in Fig. 4. The large error suggests there is no close digital material pattern in the library for some given material composition due to the limited amount of patterns in the library.
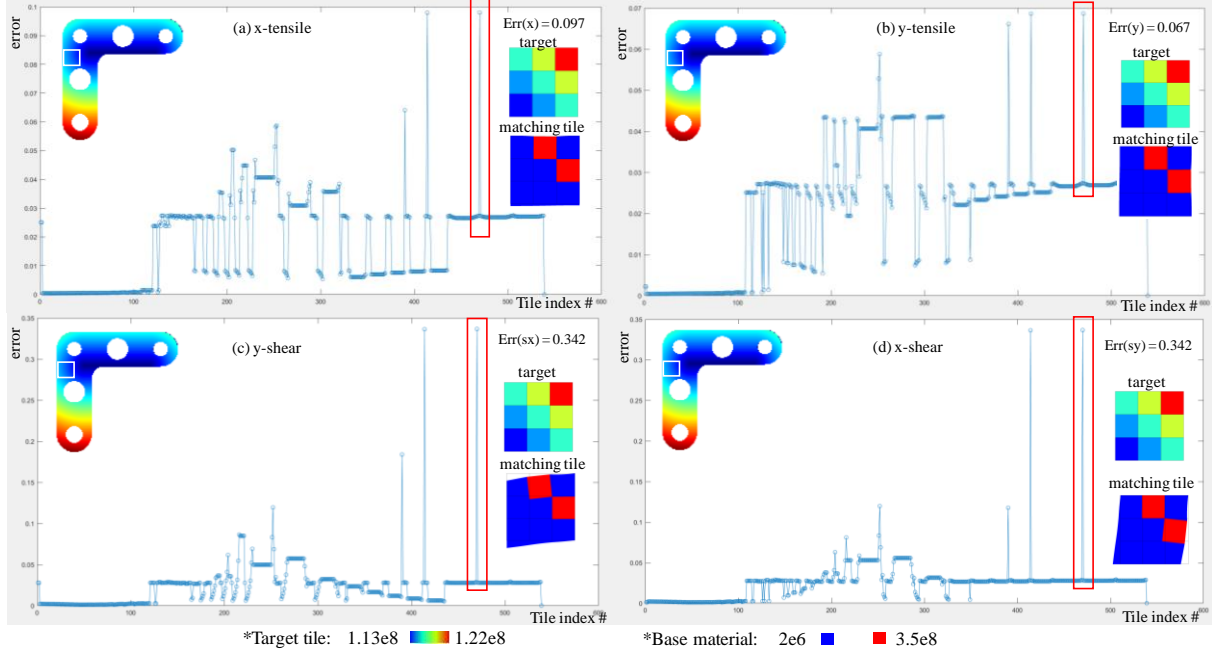
Fig. 4. An example of the similarity measures for tensors based on the tiles of a L-shaped model. One tile and the matched digital material pattern are shown with the related errors.

Error Diffusion. An approximation in each tile often comes with an error. The errors can be cumulative if they are in the same direction or compensating if they are in the opposite direction. If the errors are cumulative, they are magnified, and the overall result of a designed HO becomes too far away from the desired material property. Therefore, it is important to consider the neighboring tiles together to make sure the errors are properly compensated. Inspired by the error diffusion methods that have been widely used in 2D color printing [36], we extended the concept of half-toning in 2D color printing to 3D printing by distributing errors among neighboring tiles for the developed tensor representation.

Error diffusion is a halftoning technique that has been commonly used for image manipulation. Through the distribution of pixel quantization residual by a weight ratio to neighboring pixels, a multi-level image can be converted into a restricted level of the image (e.g., a binary image). A key difference for the error diffusion methods used in 2D color printing and the ones used in 3D printing is the basic principle and the related criteria. That is, the physical principle for 2D color printing is the gray scale levels of a printed 2D image can be visually interpolated by a human brain; in comparison, the physical principle for error diffusion in 3D printing is the material behavior under external loads and constraints should be the same.

Hence, instead of using the approach of spreading error with constant weight ratios that is generally used in 2D color printing, we divided the error into four components in the tensor-based error diffusion method. Each component represents the deformation error between two tiles that under the same loadings in a single DOF. The error components are spread individually across the domain, and each of them needs to follow the governing equation of the related physical property. For example, assuming there are two neighboring cells, c_1 and c_2. They are assigned to materials with Young's modulus E_1 and E_2, respectively. If c_1 is approximated by a Young's modulus $\overline{E_1}$, our target is to find a new value of Young's modulus $\overline{E_2}$ such that the deformation for both c_1 and c_2 after the approximation will be the same. Following the stress-deformation equation, the compensation can be governed by

$$\frac{\sigma l}{E_1} + \frac{\sigma l}{E_2} = \frac{\sigma l}{\overline{E_1}} + \frac{\sigma l}{\overline{E_2}} \tag{4}$$

where l is the length of the cells and σ is the stress applied along the x-direction. With this equation, we can understand how c_2 should be compensated to reduce the approximation error in c_1. We extend this idea to a tile with multiple Young's modulus; the performance is now not described by a simple scalar value. The tensor representation is also used to describe both the tensile and shear response along the x- and y-directions as well as the shearing behavior of multi-material tiles.

Let's define the approximation error for a tile as $\lambda = T_{target} - T_{appr}$. The target tensor T_{target} is the desired value and T_{appr} is the approximated tensor that is searched from the digital material library with the minimum distance ϵ_{sim}. Note that the components of the error $\lambda = [\Delta x \quad \Delta y \quad \Delta x_\tau \quad \Delta y_\tau]$ are independent of each other and any operations done on them are component-wise. Our goal is to produce a correction factor that will be added to the neighbouring tiles such that the total

approximation error is reduced. An example of diffusing the component Δx_τ into 3 neighbors is shown in Fig. 5. For the sake of simplicity, we only show the deformation caused by shear stress τ_x.
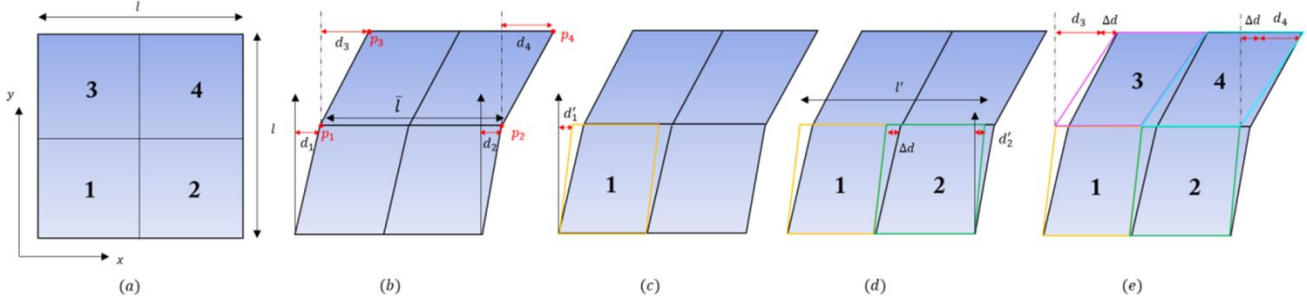
Fig. 5. Error diffusion of shear component $\boldsymbol{\Delta x_\tau}$. (a) A big tile with edge length $\boldsymbol{l}$ is formed by four 3-by-3 grids. (b) The big tile is deformed under shear stress, such that the edge length is deformed to $\bar{l}$. (c) Tile $\boldsymbol{T_1'}$ replaces the original tile with new displacement $\boldsymbol{d_1'}$. (d) In order to compensate the error $\Delta d = \boldsymbol{d_1} - \boldsymbol{d_1'}$, $\boldsymbol{T_2}$ has to deform $(\boldsymbol{d_2} - \Delta d)$ to reach to the same deformed edge length. (e) For the tiles $\boldsymbol{T_3}$ and $\boldsymbol{T_4}$, they have to move Δd to reach to the original positions of top edge.

In the first block, a tile T' from the library is used to replace the original one with the new displacement d_1'. Our goal of the diffusion operator is to maintain the same length deformation $\Delta l = \bar{l} - l$ of the line between p_1 and p_2 after the replacement. Therefore, we need to diffuse the error $\Delta d = d_1 - d_1'$ to the block 2 such that $\Delta l = (d_2 - \Delta d) - d_1'$ remains the same. The new target $d_2' = d_2 - \Delta d$ in the second tile is to compensate for the error from the first one. While for the third and fourth tiles, the shear error is diffused such that the top edge of the tiles can stay in the same position. In this way, we try to achieve a similar boundary behavior of the tiles when one of the tiles is replaced. Based on these boundary rules, we distribute other error components as depicted in Fig. 6 (left most). And the error diffusion operator ρ_{diff} can be expressed as
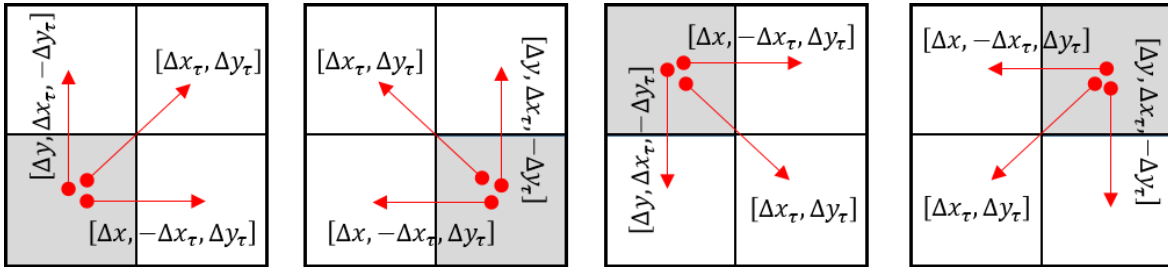
$$\rho_{diff}(T_{i+1,j}) = T_{i+1,j} + (\lambda_{i,j}^T \cdot u_x) \tag{5}$$

$$\rho_{diff}(T_{i,j+1}) = T_{i,j+1} + (\lambda_{i,j}^T \cdot u_y) \tag{6}$$

$$\rho_{diff}(T_{i+1,j+1}) = T_{i+1,j+1} + (\lambda_{ij}^T \cdot u_{xy}) \tag{7}$$

where

$$u_x = \begin{bmatrix} 1 \\ 0 \\ -1 \\ 1 \end{bmatrix}^T, u_y = \begin{bmatrix} 0 \\ 1 \\ 1 \\ -1 \end{bmatrix}^T, u_{xy} = \begin{bmatrix} 0 \\ 0 \\ 1 \\ 1 \end{bmatrix}^T.$$

Fig. 6. Diffusion inside a group of tiles. The gray tile diffuses the error λ to other white tiles, and the tensor of the white tiles will be updated for the computed compensation. The operations are performed four times in total to see which one is the best approximation for this big tile.

Each tile can either update its tensor or diffuse the error to the neighboring tiles. Updating the tensor means the current tile needs to compensate the error λ induced by its neighbors, while diffusing the error to others means current tile is the one to generate λ, and its neighbors' tensors will be updated accordingly. The algorithm starts with one initial tile $C(i,j)$ and a group of four tiles is formed by $C(i,j), C(i+1,j), C(i,j+1), C(i+1,j+1)$. To make sure the error diffusion does not have any directional bias, the tiles will be considered four in a group using the error diffusion principle as discussed in Fig. 5. For a group with four tiles , the target tensor based on the continuous material distribution of the four tiles is computed using FEA. Because there are only four update/diffusion compositions (refer to Fig. 6), instead of applying any heuristics to decide which should be updated and which should be diffused, we simply test all the four cases. For each case, we identify the digital material pattern in the library with the most similar tensor for each of the four tiles. Then we use FEA to compute the tensor for the group with replaced digital material composition. Finally the case that gives the lowest tensor approximation error is chosen as the diffusion result. After that, the process will proceed to the next tile $C(i+1,j)$ and form another group of four tiles to update the associated tensors. In other words, we determine the local diffusion for every four tiles and repeat the

operation over the entire domain. As a result, the global deformation of the computed digital material composition is capable of being approximated closely to the target one. There are special cases for the tiles on the domain boundary $\partial\Omega$ that have empty elements. As their empty elements are just filled by M_{soft} and they are the free ends, their approximation errors will not be propagated to their neighbors during the error diffusion; however, they still receive errors from their neighboring tiles. Because this method is basically a greedy algorithm, different starting points and the related sequence will lead to different diffusion results. However, due to the aforementioned selection approach among four update/diffusion compositions, the diffusion results and the related approximation errors are similar in our experimental tests. The indifference could be due to the low shape complexity of the tested models. A strategy of determining the starting point and error diffusion sequence for more complex models will be studied in our future work.

5. Results and Discussion

The proposed digital material design framework was implemented using C++. All the tests were performed on a computer with Intel i7-4790 CPU @3.60GHz and 16GB RAM. The main goal of the framework is to use only the two base materials to approximate the mechanical properties of given analog material composition. For the framework to compare the deformations between the continuous and digital materials, both simulations and physical experiments were performed under the same loading and boundary condition. All the simulation in the tests was done using FEA software COMSOL Multiphysics 5.1 on a Matlab platform. In the physical experiments, a mask-image-projection-based Stereolithography (MIP-SL) process [6] was adopted to fabricate the designed heterogeneous objects with digitally controlled multi-material deposition. The two photocurable resins selected for our experimental testing are $M_{soft} = 2MPa$ and $M_{hard} = 350MPa$. The two base materials enable one to cover a range of the input continuous Young's modulus from 2MPa to 164MPa.

For each test case, an input 3D model is sliced into 2D layers that are defined as mask images. The generated mask images are then projected onto the related photocurable resin tank to solidify the materials in the corresponding pixels selectively. For two base materials considered in a HO design, two mask images are used to specify the position of the two base materials in each layer. An example for a CAD model (refer to Fig. 9) is shown in Fig. 7. After the related material is deposited in a layer, we switch resin tanks between M_{soft} and M_{hard}, and the extra resin is cleaned after the switch. Hence for each layer of the 3D model, two mask images for both materials are generated based on the computed digital material composition. The resolution of the design domain is defined by the 3D printer's XY resolution. Each element is corresponding to a regular grid of pixels. The resolution of our 3D printer was 0.05 mm per pixel. However, it is challenging to use a single pixel size to fabricate the checkerboard type of geometry due to uncontrolled noises in environment, material, and hardware and the requirements of removing extra resin. For the sake of reliability and repeatability, we defined the size of voxels as 0.25mm, which was used in all the tests in the paper.
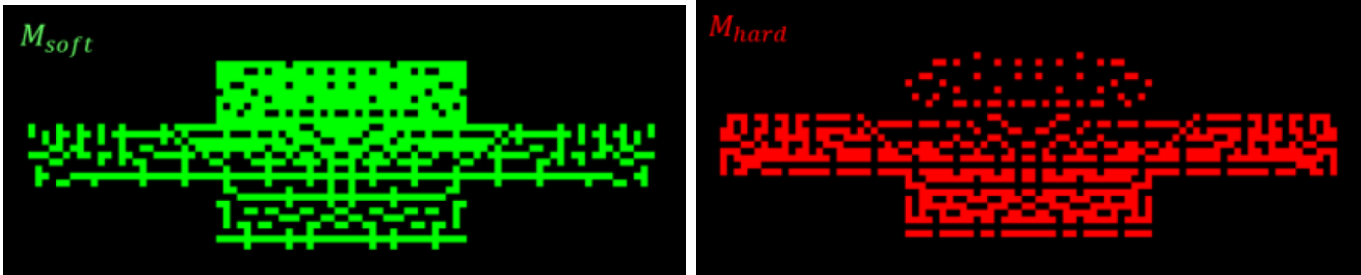

Fig. 7. Mask images generated for fabrication. The red pixels indicate the position of hard material while the green pixels refer to soft material.

5.1 Quality

To evaluate the performance of the presented design framework, we used Hausdorff distance to measure the shape error of the digital material design results. The Hausdorff distance d_H describes the maximum distance of a set to the nearest point of another set. Let $A = \{a_1, \dots, a_m\}$ and $B = \{b_1, \dots, b_n\}$ denote the mesh nodes of two models. The Hausdorff distance is defined as

$$d_H(A, B) = max\big(h(A, B), h(B, A)\big) \tag{8}$$

where $h(A, B) = \max_{a \in A} \min_{b \in B} \|a - b\|$.

In our experiments, d_H is computed to estimate the deviation of the approximation solutions. Table 1 lists the Hausdorff distance for all the test cases. We also listed the Young's modulus range E_{rng} of the given designs, the number of elements n, and the runtime performance during the online phase. In general, the results show that the approximation error is small ($<$ 0.05%) relative to the size of the domain.

Table 1. Simulation performance for various examples. The different columns show the shape deviation of the approximated designs, the Young's modulus range of the given designs, the time in minutes needed to compute the online phase and the number of elements in the domain.

Model	Fig.	d_H	E_{rng}(MPa)	T(min)	#n
Rabbit	8	0.036%	2.0-8.8	16.3	2725
Flappy	9	0.028%	2.0-16.1	7.5	1458
Slot	10 (up)	0.011%	2.0-21.3	19.5	3156
	10 (down)	0.033%	2.0-21.3	19.5	3156
Tweezers	11 (1)	0.014%	2.0-16.9	30.3	4661
	11 (2)	0.021%	2.0-164.1	30.3	4661

In Fig. 8, we show an example that the same geometry (the rabbit ears) can have different deformations under the same applied force due to different material compositions. The left ear is designed to be more rigid than the right ear. When the same force is applied to both ears, the right ear is deformed more than the left one. Similarly, Fig. 9 shows an example of a symmetrical shape with symmetrically applied loads. However, the heterogeneous material composition results in asymmetrical deformation that is non-intuitive to specify the digital material composition. The two test cases highlight the motivation for our work. For multi-material design, directly optimizing the material composition using k base materials is extremely challenging; interactively finding the right combinations as well as the right positions of where to put the base materials is also difficult for designers.
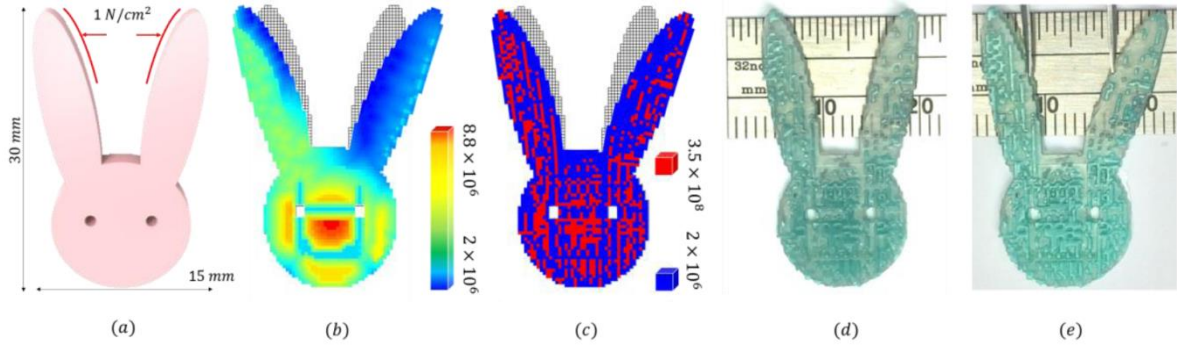

Fig. 8. (a)The rabbit model is subjected to equivalent force on the ears. (b) Desired deformation is predicted by FEA simulation. (c) A design uses two materials to approximate the deformation. (d) Physical test of the fabricated model. (e) The actual deformations are consistent with the predicted result.
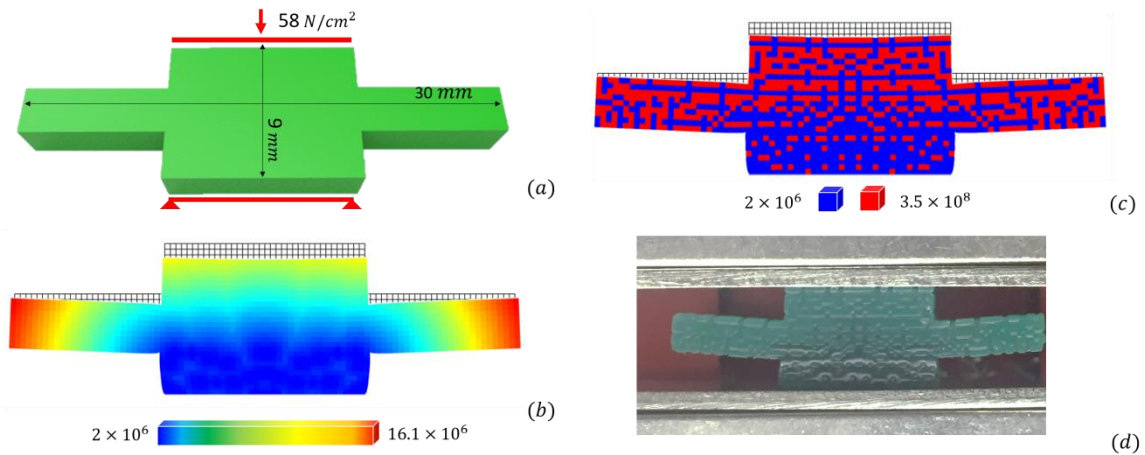
Fig. 9. (a) Flappy CAD model. (b) Predicted deformation with the analog material distribution. (c) Predicted deformation with approximation solution. The result shows that the framework can approximate accurately the behavior using two materials. (d) Fabricated model and its deformation result.

The L-shape slot shown in Fig. 10 is a more complex example with internal holes. It also demonstrates that our approach is not force-oriented. As shown in Fig. 10, two forces are applied to different locations in each design. Their deformation behaviors are similar in both the approximated and continuous material distributions. The test case shows that the presented tensor representation is general and able to approximate the desired material properties for two or more specified deformations. Finally, the tweezers in Fig. 11 demonstrates a robotic grasper whose design can benefit from our multi-material design

framework. In the test case, we studied the displacement at the tipping point of the tweezers (yellow dot) under various loading conditions to verify the impact of different applied forces on the accuracy of the deformation behaviors of different designs. A similar force-displacement relationship is observed in the target and the approximation results. The errors of one of the tweezers designs (Design 1) are summarized in Table 2. We report the shape deviations in terms of Hausdorff distance. More details of the physical experiments for the tweezers case are shown in Appendix A.
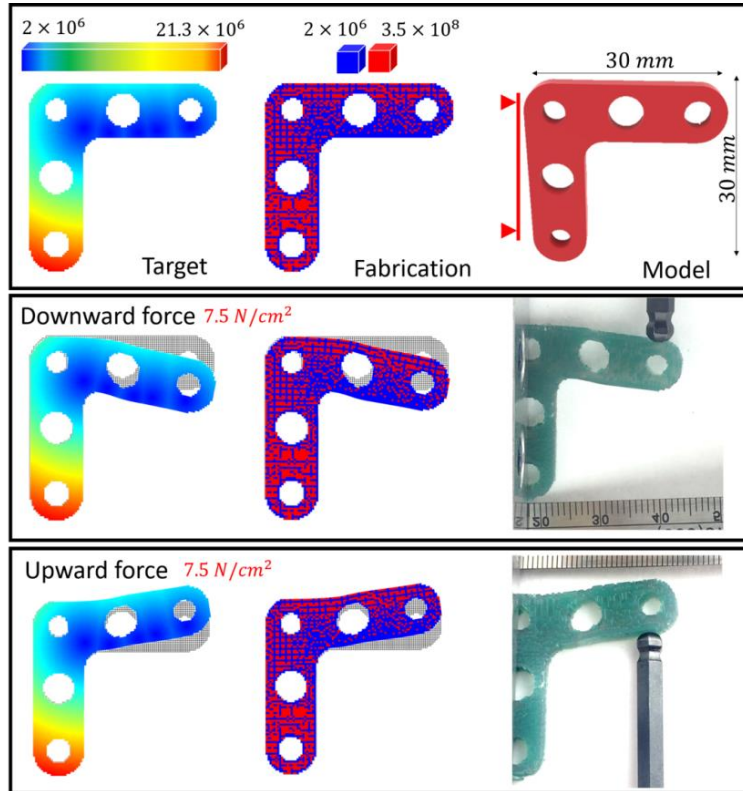

Fig. 10. Two forces are applied to the L-shape slot model. The results show that the solution is able to approximate the material properties instead of specific deformations.

Table 2. Hausdorff distance of the approximated tweezers (Design 1 in Fig. 11) under various loads.

Force (N/cm^2)	d_H
0.05	0.003%
0.13	0.007%
0.20	0.009%
0.27	0.013%
0.45	0.021%
0.69	0.033%

We also compared the deformation of the tweezers subjected to $0.27\ N/cm^2$ in the single material and multi-material designs. As shown in Fig. 11, two multi-material tweezers designs possess mechanical properties that are between the two single material designs, which suggest the proposed multi-material approach can generate a range of configuration solutions for more complex deformation behaviours under the same load. Thousands of possible heterogeneous designs can be incorporated in more complex product components that were previously impossible to design and fabricate. All the test cases show that our design framework is general for various geometric shapes and material variations.
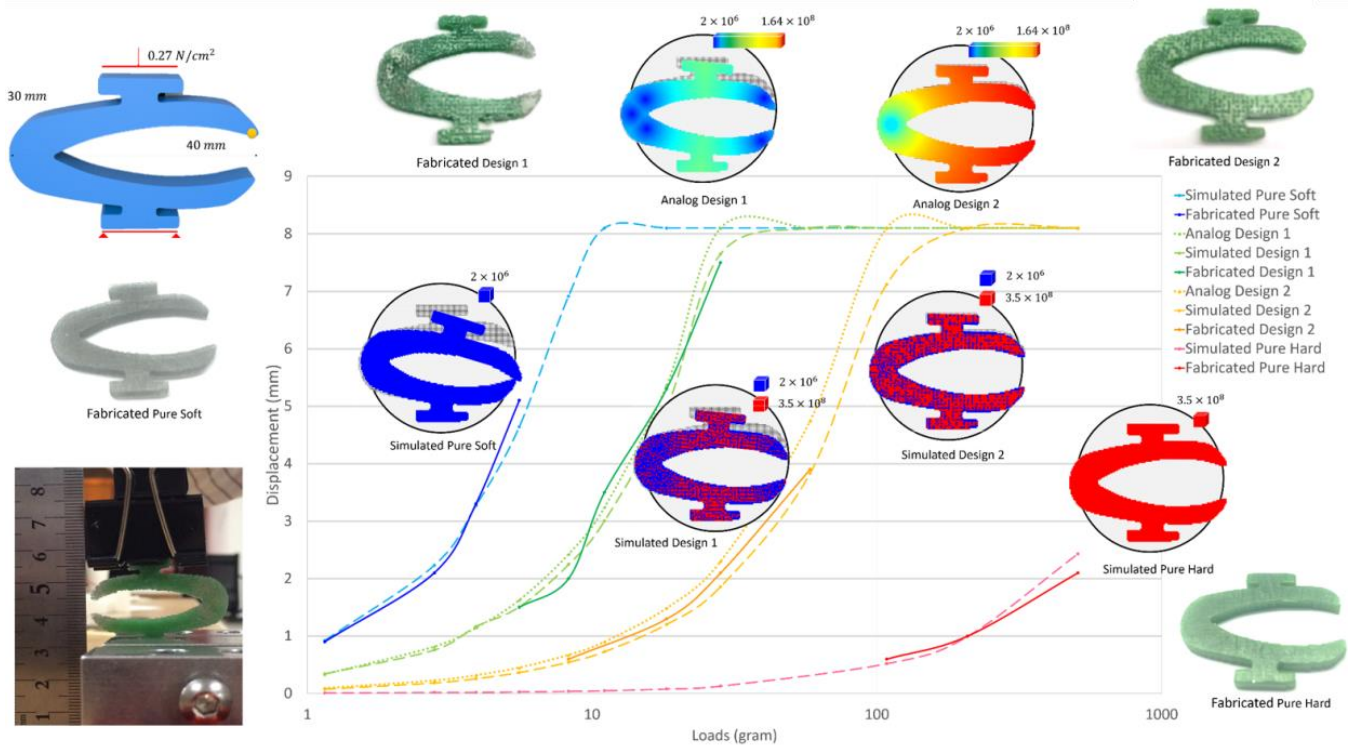
Fig. 11. An example of multi-material tweezers models demonstrates the ability to convert designs with target deformations into real products for additive manufacturing. Force and displacement relationship are plotted for the target and approximation designs, in addition to the single material designs. Both the simulation and physical experiment results proved that the proposed method could provide good approximations for input analog material compositions, regardless of their geometric shape and material variations.

5.2 Performance

While the primary focus of our study is the effectiveness of the computed multi-material solutions, we discuss the efficiency of our approach in the section. From the computation point of view, the framework can be divided into three phases: library construction, input analysis, and error diffusion (refer to Fig. 1). The computation of the first two phases mainly relies on the finite element simulation using COMSOL. To extract a tensor from one tile, the finite element analysis needs to be performed four times with different force conditions, which takes around ~2.2 seconds in total. Since we need to extract 512 tensors for all the patterns in a digital material library, this could require around 20 mins in the library construction phase. Compared with the optimization method for designing microstructures [21], it took around 2 hours to converge per structure with about 4000 elements, and there is an error of 0.6% - 2.5% between the predicted and the measured results. For the second and third phases, the performance depends on the number of tiles, which is related to the input geometric shape and element sizes. Table 1 lists the number of elements for all the test cases. For example, in the tweezers model, extracting the tensors from the input analog material takes around 30 mins, while the error diffusion takes about 13 seconds. It can be seen that the error diffusion phase is very fast compared with the other two phases. The main bottleneck of the framework is the communication of our software with COMSOL during the process of extracting tensor. In the future, we will implement an integrated FEA solver to reduce the computation overhead in the current implementation.

6. Conclusions and Future Work

In summary, we have presented a novel digital material design framework to generate heterogeneous objects with user-specific behavior. The computed heterogeneous objects can then be printed by multi-material additive manufacturing processes. Our work provides a solid foundation on how to utilize multi-materials to achieve specified mechanical properties, and how to ensure the solution can be manufactured by the current 3D printing technology. While most AM processes have limited base materials that can be printed, a heterogeneous object that can now be 3D-printed may still have a design space that is too large to explore. It is difficult to directly optimize the digital material composition in a given design domain due to the exponentially increased degrees of freedom. Our proposed framework offers a promising path on generating digital materials that are 3D-printable and, at the same time, meet the given design requirements. We have performed both simulation and physical experiments to validate the design framework for multiple test cases. The results show good consistency between the simulation

and the physical test results. Our framework is also general and can be scalable to support more than two materials as well as including Poisson's ratio as a design parameter.

In our future work, we plan to extend the work from 2D to 3D using a similar principle. That is, the tile in 3D cases would be a cubic of size $3 \times 3 \times 3$; and for the behavior of the cubic tile, the tensor should include the deformations subjected to forces along the x, y, z directions and in three shearing planes. Accordingly, the digital material library for 3D cases needs to be expanded dramatically with the number of patterns to be $2^{3 \times 3 \times 3}$. Although the idea seems straightforward, the computation will be significantly increased. Hence a data-driven approach with compression technique may be considered in our future work to reduce the searching and matching complexity. We also plan to extend the framework for an increased number of grids such as 4-by-4 or 5-by-5 elements as well as different loading conditions. Similarly, the required computation will be significantly increased as well.

Acknowledgements

References

[1]   W. Gao, Y. Zhang, D. Ramanujan, K. Ramani, Y. Chen, C. Williams, C. Wang, Y. Shin, S. Zhang and P. Zavattieri, "The status, challenges, and future of additive manufacturing in engineering," *Computer-aided Design,* vol. 69, pp. 65-89, 2015.

[2]   Y. Yang, X. Song, X. Li, Z. Chen, C. Zhou, Q. Zhou and Y. Chen, "Recent progresses in biomimetic additive manufacturing technology: from materials to functional structures," *Advanced Materials,* vol. 30, p. 1706539, 2018.

[3]   H. Yuna, V. Y. Blouin and M. F. Georges, "Incorporating manufacturability constraints into the design process of heterogeneous objects," *Proceedings of the SPIE,* vol. 5605, pp. 214-225, 2004.

[4]   U. Hejmadi and K. McAlea, "Selective laser sintering of metal molds: the rapid tool process," in *Solid Freeform Fabrication Symposium*, Texas, August 12th-14th, 1996.

[5]   Y. F. Zhu, C. Peng, J. Q. Yang and C. M. Wang, "An Integrated Design and Fabrication Approach for Heterogeneous Objects," *Advanced Materials Research,* Vols. 383-390, pp. 5810-5817, 2012.

[6]   C. Zhou, Y. Chen, Z. Yang and K. Behrokh, "Digital material fabrication using mask-image-projection-based stereolithography," *Rapid Prototyping Journal,* vol. 19, no. 3, pp. 153-165, 2013.

[7]   Y. Miyamoto, W. A. Kaysser, B. H. Rabin, A. Kawasaki and R. G. Ford, Functionally Graded Materials: Design, Processing and Applications, Boston: Kluwer Academic Publishers, 1999.

[8]   J. Hiller and H. Lipson, "Design and analysis of digital materials for physical 3D voxel printing," *Rapid Prototyping Journal,* vol. 15, no. 2, pp. 137-149, 2009.

[9]   P. Huang, Y. Li, Zeng, Y. Chen and Jun, "A digital material design framework for 3D-printed heterogeneous objects," in *ASME International Design Engineering Technical Conferences and Computers and Information in Engineering Conference*, 2016.

[10] H. Xu, Y. Li, Y. Chen and J. Barbic, "Interactive material design using model reduction," *ACM Trans. Graph.,* vol. 34, pp. 18:1-18:14, 2015.

[11] M. Ashby, "Materials and shape," *Acta Metallurgica et Materialia,* vol. 39, no. 6, pp. 1025-1039, 1991.

[12] O. Sigmund, "Tailoring materials with prescribed elastic properties.," *Mechanics of Materials,* vol. 20, no. 4, pp. 351-368, 1995.

[13] S. Zhou and Q. Li, "Design of graded two-phase microstructures for tailored elasticity gradients," *Journal of Materials Science,* vol. 43, p. 5157, 2008.

[14] G. Allaire, Shape Optimization by the Homogenization Method, Springer Science & Business Media, 2002.

[15] X. Huang, A. Radman and Y. Xie, "Topological design of microstructures of cellular materials for maximum bulk or shear modulus," *Computational Materials Science,* vol. 50, no. 6, pp. 1861-1870, 2011.

[16] M. P. Bendsoe, "Generating optimal topologies in structural design using a homogenization method," *Computer Methods in Applied Mechanics and Engineering,* vol. 71, no. 2, pp. 197-224, 1988.

[17] M. P. Bendsoe and O. Sigmund, Topology Optimization: Theory, Methods, and Applications, Springer Science & Business Media, 2003.

[18] J. Sethian and A. Wiegmann, "Structural boundary design via level set and immersed interface methods," *Journal of*

Computational Physics, vol. 163, no. 2, pp. 489-528, 2015.

[19] T.-H. Kwok, Y. Li and Y. Chen, "A structural topology design method based on principal stress line," *Computer-aided Design,* vol. 80, pp. 19-31, 2016.

[20] B. Bickel, M. Bacher, M. A. Otaduy, H. R. Lee, H. Pfister, M. Gross and W. Matusik, "Design and Fabrication of Materials with Desired Deformation Behavior," *ACM Trans. Graph.,* vol. 29, pp. 63:1-63:10, 2010.

[21] C. Schumacher, B. Bickel, J. Rys, S. Marschner, C. Daraio and M. Gross, "Microstructures to control elasticity in 3D printing," *ACM Trans. Graph.,* vol. 34, pp. 136:1-136:13, 2015.

[22] J. Panetta, Q. Zhou, L. Malomo, N. Pietroni, P. Cignoni and D. Zorin, "Elastic Textures for Additive Fabrication," *ACM Trans. Graph.,* vol. 34, pp. 135:1-135:12, 2015.

[23] B. Zhu, M. Skouras, D. Chen and W. Matusik, "Two-Scale Topology Optimization with Microstructures," *ACM Trans. Graph.,* vol. 36, no. 5, pp. 164:1-164:16, 2017.

[24] T. Jackson, H. Liu, N. Patrikalakis, E. Sachs and M. Cima, "Modeling and designing functionally graded material components for fabrication with local composition control," *Material & Design,* vol. 20, no. 2-3, pp. 63-75, 1999.

[25] W. Chiu and K. Yu, "Direct digital manufacturing of three-dimensional functionally graded material objects," *Computer Aided Design,* vol. 40, no. 12, pp. 1080-1093, 2008.

[26] H. Liu, T. Maekawa, N. Patrikalakis, E. Sachs and W. Cho, "Methods for feature-based design of heterogeneous solids," *Computer Aided Design,* vol. 36, no. 12, pp. 1141-1159, 2004.

[27] K. Samanta and B. Koc, "Feature-based material blending for heterogeneous object modeling," *Computer Aided Design,* vol. 37, no. 3, pp. 287-305, 2005.

[28] X. Qian and D. Dutta, "Feature-based design for heterogeneous objects," *Computer Aided Design,* vol. 36 , no. 12, pp. 1263-1278, 2004 .

[29] D. S. Schnur and N. Zabaras, "An inverse method for determining elastic material properties and a material interface," *International Journal for Numerical Methods in Engineering,* vol. 33, no. 10, pp. 2039-2057, 1992.

[30] M. Becker and M. Teschner, "Robust and Efficient Estimation of Elasticity Parameters using the Linear Finite Element Method," in *Simulation und Visualisierung*, 2007.

[31] B. Bickel, M. Bacher, M. A. Otaduy, W. Matusik, H. Pfister and M. Gross, "Capture and Modeling of Non-linear Heterogeneous Soft Tissue," *ACM Trans. Graph.,* vol. 28, no. 3, pp. 89:1-89:9, 2009.

[32] Q. Lou and P. Stucki, "Fundamentals of 3D halftoning," in *Electronic Publishing, Artistic Imaging, and Digital Typography*, Berlin, Heidelberg, Springer, 1998, pp. 224-239.

[33] E. Doubrovski, E. Tsai, D. Dikovsky, J. Geraedts, H. Herr and N. Oxman, "Voxel-based fabrication through material property mapping: A design method for bitmap printing," *Computer Aided Design,* vol. 60, pp. 3-13 , 2015.

[34] W. Cho, E. M. Sachs, N. M. Patrikalakis and D. E. Troxel, "A dithering algorithm for local composition control with threedimensional printing," *Computer Aided Design,* vol. 35, no. 9, pp. 851-867, 2003.

[35] K. Vidimče, S.-P. Wang, J. Ragan-Kelley and W. Matusik, "Openfab: A programmable pipeline for multi-material fabrication," *ACM Transactions on Graphics (TOG),* vol. 32, no. 4, 2013.

[36] L. Kharevych, P. Mullen, H. Owhadi and M. Desbrun, "Numerical Coarsening of Inhomogeneous Elastic Materials," *ACM Trans. Graph.,* vol. 28, pp. 51:1-51:8, 2009.

[37] R. W. Floyd and L. Steinberg, "An Adaptive algorithm for spatial grey scale.," *Proceedings of the Society of Information Display,* pp. 17, 75–77, 1976.

Appendix A. Physical Experiment of the Tweezers Case

Physical experiments (see Fig. 12) were conducted to verify the performance of the multi-material designs. We measured and plotted the displacement of the tweezers tip point against the predicted displacements from the FEA simulation. Four fabricated tweezers were tested using a soft material, a hard material, and two mixtures of the two base materials that were generated by our design framework. In the first and second experiments, we hypothesized the Young's modulus of the soft and hard materials. The simulation result for the third and fourth experiments are acquired based on the hypothesized results. By comparing the measured and predicted performance of the tweezers designs, it can be observed that the response of the 3D-printed objects is closely matched to the predicted one. The discrepancy between the tested and predicted results is also shown in the plots, which could be caused by measuring and manufacturing errors. Overall, the experiments verify the effectiveness of

the presented multi-material design approach.
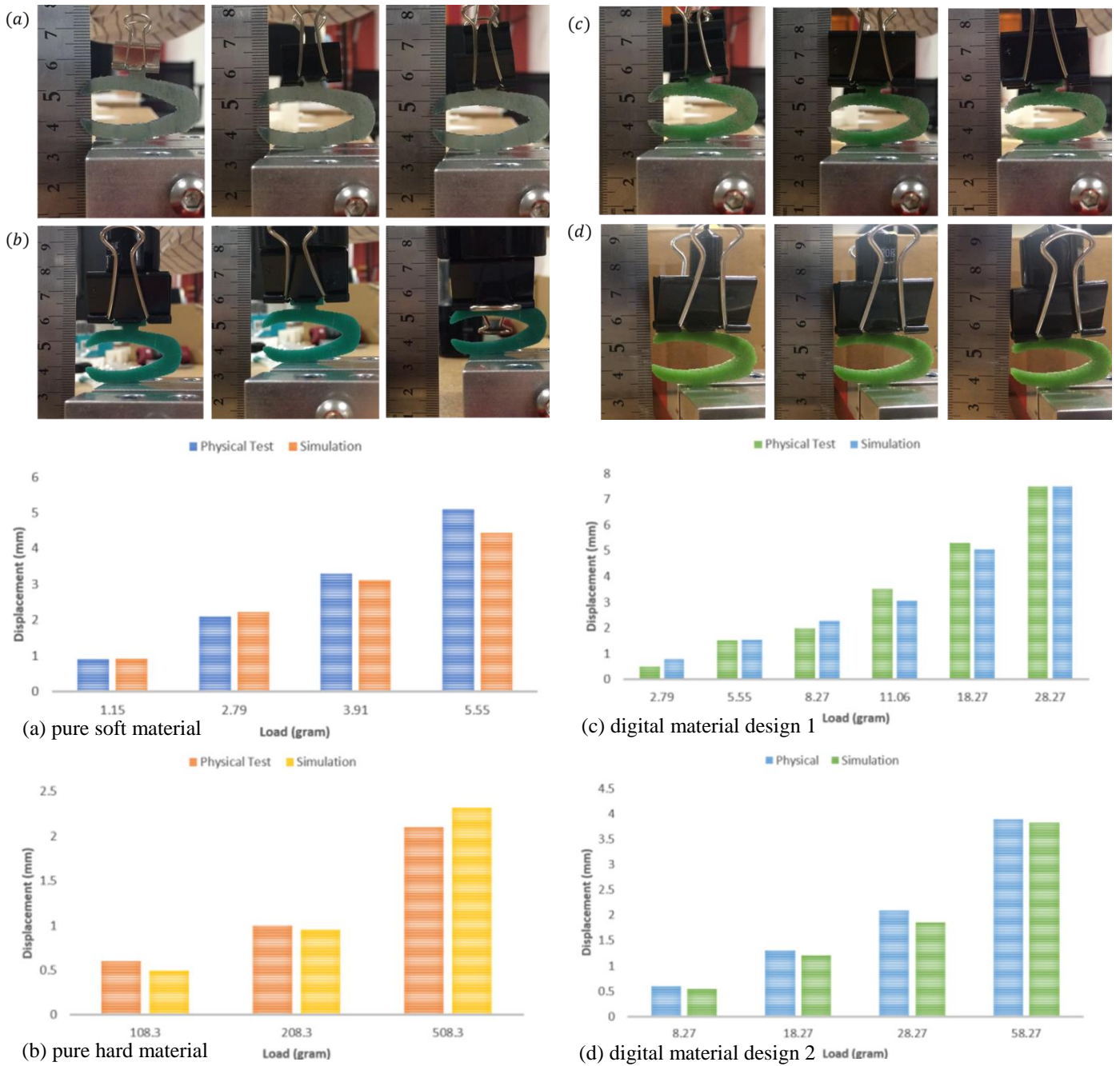
Fig. 12. Physical setup for the experiments. (a) Tweezers fabricated in pure soft material. (b) Tweezers fabricated in pure hard material. (c)(d) Tweezers fabricated with two materials as designed in Fig. 11. A comparison between the actual and the predicted deformation values is plotted, with some minor discrepancy that is probably due to measuring and manufacturing errors.